PHOTONICS Research

Sum-frequency generation in on-chip lithium niobate microdisk resonators

Zhenzhong Hao,[1] Jie Wang,[1] Shuqiong Ma,[1] Wenbo Mao,[1] Fang Bo,[1,2,*] Feng Gao,[1,2] Guoquan Zhang,[1,2,3] and Jingjun Xu[1,2,4]

[1]The MOE Key Laboratory of Weak Light Nonlinear Photonics, TEDA Institute of Applied Physics and School of Physics, Nankai University, Tianjin 300457, China
[2]The Collaborative Innovation Center of Extreme Optics, Shanxi University, Taiyuan, Shanxi 030006, China
[3]e-mail: zhanggq@nankai.edu.cn
[4]e-mail: jjxu@nankai.edu.cn
*Corresponding author: bofang@nankai.edu.cn

Received 27 July 2017; revised 13 September 2017; accepted 13 September 2017; posted 22 September 2017 (Doc. ID 302366); published 31 October 2017

We report the first observation, to the best of our knowledge, of sum-frequency generation in on-chip lithium niobate microdisk resonators. The sum-frequency signal in the 780 nm band, distinct in wavelength from second-harmonic signals, was obtained in lithium niobate microresonators under the pump of two individual 1550 nm band lasers. The sum-frequency conversion efficiency was measured to be 1.4×10^{-7} mW^{-1}. The dependence of the intensities of the nonlinear signals on the total pump power and the wavelength of one pump laser was investigated while fixing the wavelength of the other. This work paves the way for applications of on-chip lithium niobate microdisk resonators ranging from infrared single-photon detection to infrared spectroscopy.

OCIS codes: (140.3945) Microcavities; (130.3730) Lithium niobate; (190.0190) Nonlinear optics; (230.5750) Resonators.

https://doi.org/10.1364/PRJ.5.000623

1. INTRODUCTION

Whispering gallery mode (WGM) microresonators with high quality (Q) factors and small mode volume have abilities to dramatically boost light-material interactions. They find applications ranging from ultrasensitive sensing [1–3] to low-threshold lasing [4]. They also provide a platform for fundamental studies, such as nonlinear optics [5–10], cavity quantum electrodynamics [11], optomechanics [12,13], PT symmetry [14,15], and topological photonics [16].

In comparison with Fabry–Perot and photonic crystal microcavities, WGM microresonators allow simultaneous resonances at very different wavelengths due to light confinement via total internal reflection. WGM microresonators can obtain high-Q in the whole transparent window of the material that is employed to make the microcavity. As a result, WGM microresonators are natural candidates for investigations and applications of nonlinear optical effects associated with different wavelengths [6,7,9,10].

Nonlinear optical effects associated with multiple wavelengths with low power pumps can be realized in multiple-resonance WGM resonators with high Q factors. Third-order nonlinear effects, such as stimulated Raman scattering [4], stimulated Brillouin scattering [17], and four-wave mixing [18,19] were reported in silica, calcium fluoride, and silicon nitride microresonators. The common feature of these materials is possessing central symmetry. Therefore, under the dipole approximation, the lowest order of nonlinear effects in these materials is the third order, which provides the possibility to realize optical comb [19] and nonreciprocal light transmission [17,18] in WGM microresonators.

Second-order nonlinear optical effects were mainly realized in microcavities made from materials such as lithium niobate (LN) [6–10], lacking central symmetry. As a well-known versatile nonlinear optical medium, LN has second-order nonlinear properties with $\chi^{(2)}$ as high as 41.7 pm/V. Nonlinear optical effects such as second-harmonic generation (SHG) [6,7], sum-frequency generation (SFG) [8], and optical parametric oscillation (OPO) [9,10] were intensively explored in millimeter-sized LN WGM resonators fabricated by diamond polishing.

Benefiting from progress in micro-fabrication techniques, on-chip LN WGM microresonators were fabricated by several groups [20–25]. The highest measured Q of LN WGM cavities on a chip can be higher than one million [25]. SHG [23,26–28] and parametric downconversion (PDC) [29] were demonstrated in on-chip LN microresonators. Electrooptic

[25,30], thermooptic [31,32] and optomechanical effects [33] were reported as well in LN microdisk resonators.

Compared with SHG [23,26–28] and optical PDC [29], SFG has the ability to efficiently covert low-frequency weak light down to single photon to high-frequency light with the aid of a strong pump. Therefore, it is widely used in the detection of infrared signals lacking cheap and efficient photodetectors by converting them into visible light that can be efficiently monitored with cost-effective detectors. Although SFG was reported in millimeter-sized LN WGM resonators not suitable for integration [8], the realization of SFG effect in on-chip LN microdisks is still a challenging task due to the difficulties in producing high-Q on-chip LN resonators and their dramatically decreased mode density.

In this paper, we report the first observation of SFG in LN microdisk cavities on a chip. The 780 nm band SFG signal, usually together with SHG signals, was generated by pumping the LN resonator with two individual lasers working in communication band. The influences of various experimental conditions on the intensity and wavelength of nonlinear optical signals were studied systematically.

2. SAMPLES AND EXPERIMENTAL SETUPS

SFG experiments were performed in an LN microdisk resonator of 40 μm radius and 500 nm thickness. The resonator was fabricated from an LN on insulator (LNOI) chip produced by NANOLN by using UV lithograph, reactive ion etching, and hydrogen fluoride wet etching in turn [25]. The quality factors in 1550 and 780 nm bands of the resonator that we used were measured to be 3.7×10^5 and 3.1×10^5, respectively.

The experimental setup for the SFG experiment is illustrated in Fig. 1. Light from a picosecond (ps) laser and that from a continuous wave (cw) laser were launched into a 50:50 fiber combiner after passing through individual polarization controllers. Both of the two lasers are working in 1550 nm band serving as pumps. Most energy of the pumps (99%) was sent to a tapered fiber made by thermally pulling a 1550 nm single-mode fiber and then partially coupled into the LN microdisk; the other 1% was detected by a power meter to measure the pump power. The light transmitted and coupled into the tapered fiber from the LN resonator was then split into two beams by using a 1550 nm 90:10 fiber splitter. The 90% port was sent into a grating spectrometer to detect the upconversion signals, while the output of the 10% port was received by an infrared photodetector to measure the quality factors of the resonator and to monitor the coupling between the tapered fiber and the resonator. The wavelength of the cw laser can be scanned forward and backward by applying a sawtooth voltage generated from an arbitrary function generator. The sawtooth voltage serves also as the trigger signal for the oscilloscope.

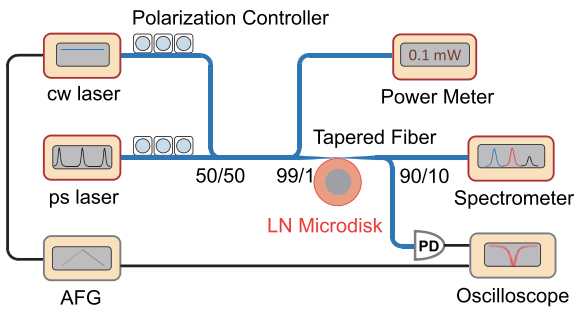

Fig. 1. Illustration of the experimental setup for investigation of nonlinear effects in LN microdisks. AFG, arbitrary function generator; PD, photodetector.

In order to efficiently and simultaneously couple the pump beams in the 1550 nm band and nonlinear signals in the 780 nm band into and out of the LN resonator, a tapered fiber with relatively thinner diameter was employed. The waist diameter of the tapered fiber was less than 2 μm. The position of the tapered fiber with respect to the LN microdisk was optimized to maximize the SFG signal. We found that, when the SFG signal reaches its maximum value, plenty of modes with quality factors extending for several orders are efficiently or even overcoupled. Additionally, the resonance dips in the transmission spectrum were broadened and shifted to the longer wavelengths due to the thermal effect and the increase in effective refractive index induced by the introduction of the coupling tapered fiber. The distortions in transmission spectrum bring us difficulties in finding the quantum numbers of the WGMs regarding the nonlinear optical process. The WGM quantum numbers are usually obtained by comparing the theoretical resonance wavelengths of the eigenmodes of the resonator in the absence of the tapered fiber to the measured spectrum in a weak coupling condition rather than in the strong coupling regime.

3. EXPERIMENTAL RESULTS AND DISCUSSIONS

We first incident one light beam from either the ps laser or the cw laser into the LN microdisk while slowly scanning the laser wavelength. When the input wavelength matches the resonance of the resonator and thus its second harmonics, we observed a second-harmonic signal from the grating spectrometer. Figures 2(a) and 2(b) show the typical second-harmonic signals with pulse and continuous pumps, whose transmission versus time is shown in Figs. 2(d) and 2(e), respectively. Then, we simultaneously sent both the ps laser and the cw laser into the microdisk. Sum-frequency signal with a frequency distinguished from the second harmonic of either pump was observed and is shown in Fig. 2(c) as an example. In this situation, the transmission of the tapered fiber coupled to LN microdisk is the algebraic sum of the two pumps, as demonstrated in Fig. 2(f). It is worth noting that the ~2 nm linewidths of the SFG and SHG signals are just the readouts of the spectrometer when we placed at its entrance a relative broad slit, with which the nonlinear optical signal can be found more easily. Such a broad linewidth is not the actual value for the nonlinear signals from a high-Q microresonator. The true value determined by the linewidth of the LN microdisk resonator was confirmed by narrowing the slit to be less than the detection limit 0.2 nm of the employed spectrometer. Note that the measured nonlinear conversion efficiency was not influenced by the slit width because the spectrometer was always calibrated after the width of the slit was changed.

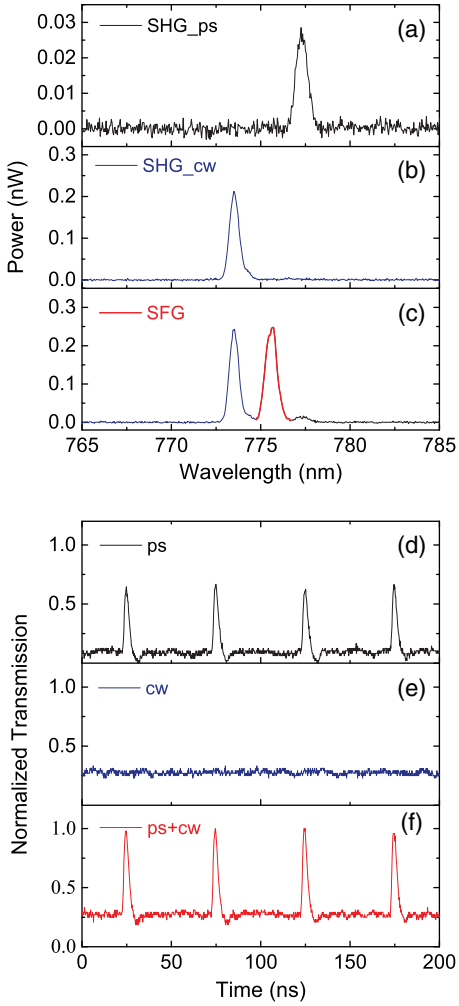

Fig. 2. Spectra of nonlinear optical signals and the corresponding transmission of the pump. SHG signals of (a) pulsed and (b) cw pumps, respectively. (c) SFG (red bold line) and SHG signals (blue and black lines) obtained when both cw and pulsed pump lasers were coupled into the LN resonator. (d)–(f) Typical transmission of the pump correspond to (a)–(c), respectively. The wavelengths (input power) of the cw and pulsed lasers were 1547.0 and 1554.6 nm (8.02 and 0.52 mW), respectively.

We found that a series of the SFG signals show up, when the wavelength of the cw pump is tuned to a broad spectral range with the ps laser wavelength fixed. In experiments, we notice that, within a spectral range from 769.3 to 777.4 nm, the SFG signal arises more than 30 times. The average distance in wavelength between two adjacent SFG frequencies is about 0.28 nm, which is much smaller than the free spectrum range ~4.6 nm of the LN microdisk used in our experiment. This phenomenon reveals that WGMs with different quantum numbers are involved in the SFG process. As an example, five upconversion signal spectra labeled as n, which range from 1 to 5, are shown in Fig. 3. The peaks in red in Fig. 3 stand for SFG signal, the blue is for SHG of the cw laser, and the black indicates SHG of the ps laser. In order to clearly show different signals, the vertical coordinates of the nth spectrum in Fig. 3 are shifted by $(n-1) \times 30$ pW. The intensities of nonlinear optical

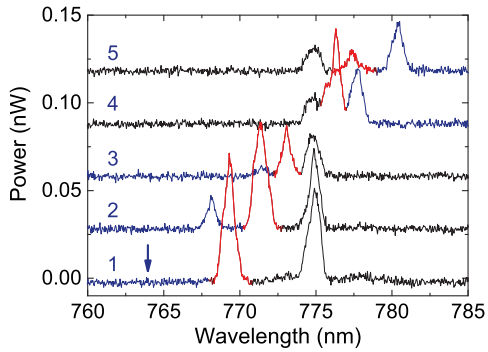

Fig. 3. Spectra showing nonlinear optical signals for various cw laser wavelengths. The red, blue, and black peaks represent the SFG, SHG of cw laser, and SHG of pulsed laser, respectively. For demonstration, the vertical coordinate for each spectrum is shifted by 10 pW with respect to its preceding one. The wavelength of the pulsed pump was fixed at 1549.7 nm. The input power of the cw and pulsed pumps were set to be 7.81 and 0.51 mW, respectively.

signals depend on various factors including the spatial overlap of the involved WGMs and the overlap of the frequencies of the pump and signal beam with the resonances of the resonator. Therefore, the intensities of SFG and SHGs fluctuate dramatically, as shown in Fig. 3. Particularly, only the SFG signal and SHG of ps laser were observed in line 1; SHG of the cw laser, which should appear in the position indicated by the black arrow, did not arise. The disappearance of SHG of the cw pump indicates its wavelength is off-resonance.

When the wavelength of the ps laser is fixed at a particular value with a maximum SHG, and the cw laser wavelength is scanned around a resonance wavelength of the LN microdisk, the change in intensities of the SHG and SFG signals with respect to the frequency detuning of the cw laser is shown in Figs. 4(a)–4(c). The SHG of the cw laser and SFG signal reach their respective maximums when the continuous laser passes through the resonances of the microdisk. The maximum nonlinear signal is the consequence of the resonance enhancement of the pump intensity within the resonator under the phase-match condition, which increases the nonlinear conversion efficiency. In contrast, the SHG of the ps laser has a minimum conversion [Fig. 4(a)] because of the resonance wavelength shift of the LN microdisk due to the thermal effect under strong pump and the competition for pump energy between the SFG and SHG signals. Significant thermal effects are clearly seen from the observed transmission spectrum under strong pump condition, as shown in Fig. 4(e) in comparison with Fig. 4(f), which is the corresponding transmission spectrum measured under weak pump condition. These transmission spectra were detected while scanning the wavelength of the cw pump by applying a sawtooth voltage, as shown in Fig. 4(d). The transmission spectrum in the presence of a weak pump obviously shows that three individual modes contribute to the nonlinear optical process, which results in the step changes and the multiple maximums in Figs. 4(a)–4(c).

The dependence of the SFG on the pump power was also investigated. The input power of both the cw and pulsed

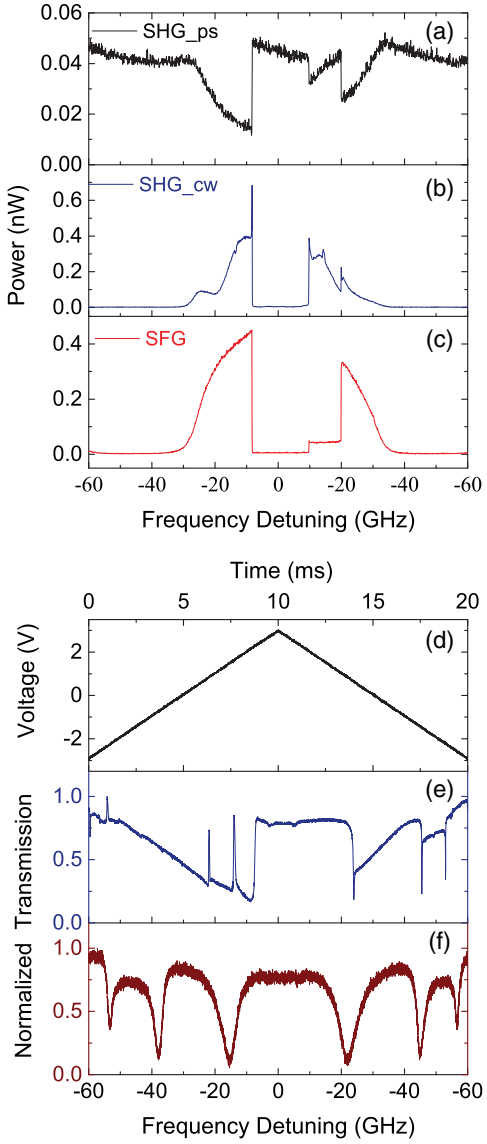

Fig. 4. Dependence of the SFG and SHG intensities on the wavelength of the cw pump and transmission spectra of the cw pump. (a)–(c) Nonlinear signals measured by scanning the wavelength of the cw laser near 1547.0 nm. The wavelength of the pulsed pump was fixed at 1554.6 nm. The input power of the cw and pulsed pumps were set to be 10.92 and 0.71 mW, respectively. (d) Sawtooth voltage for cw laser wavelength scan. Transmission spectra of the cw laser around 1543.0 nm under (e) strong and (f) weak pump, respectively.

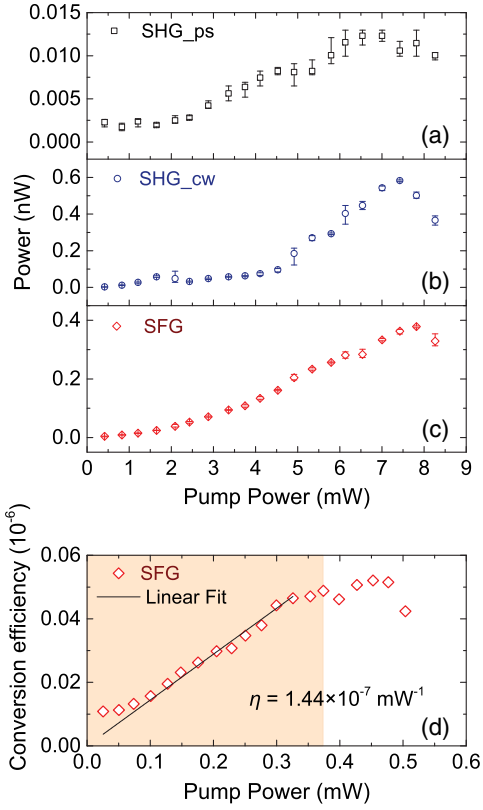

Fig. 5. Dependence of nonlinear signals on pump power and the deduced SFG conversion efficiency. (a)–(c) Power of SHG signals of the cw and pulsed lasers and SFG signal with respect to the total pump power. (d) SFG conversion efficiency deduced from (c). The central wavelengths of the cw and ps lasers were set as 1547.0 and 1554.6 nm, respectively. The power ratio of the continuous laser and the pulsed laser was kept as 15.4:1.

pumps was tuned simultaneously by using a tunable attenuator after the 50:50 combiner (not shown in Fig. 1). Figure 5 demonstrates the intensity of the SFG and SHGs as functions of the sum of the cw- and pulsed-laser power, which were measured when the central wavelengths of the cw and ps lasers were set as 1547.0 and 1554.6 nm, respectively. As shown in Figs. 5(a)–5(c), the intensities of the SFG and the SHGs increase first and then reach a maximum when total input power rises from less than 1 to 8 mW.

The SFG conversion efficiency is defined as $P_{SFG}/(P_{cw}P_{ps})$, where P_{SFG}, P_{cw}, and P_{ps} are the power of the SFG signal, the cw pump, and the ps pump, respectively. Figure 5(d) shows the ratio of SFG signal power to the cw pump power as a function of the ps pump power. An SFG conversion efficiency of 1.4×10^{-7} mW^{-1} was achieved by fitting the data in the yellow region of Fig. 5(d), which was measured in the unsaturated situation. According to the reported conversion efficiency for SHG in on-chip LN microdisks, the conversion efficiency of SFG in on-chip LN microdisks can be improved at least by 4 orders of magnitude to 10^{-3} mW^{-1} [27,28]. Theoretically, conversion efficiency can reach 100% [34]. To improve the inner conversion efficiency, the dispersion of the LN microdisk should be precisely designed by optimizing the disk geometry structure, including the thickness and radius to fulfill phase matching for fundamental modes. The employment of lasers with linewidth narrower than the WGMs will help us to improve the pump efficiency. The extraction efficiency and the measured total conversion efficiency can be improved by using an add–drop coupling system consisting of two tapered fibers to couple the pump and the signal individually.

We also investigated the impact of the pump power contributed only by the cw laser on the intensities of the nonlinear signals, while fixing the wavelength and pump power of the ps laser. In this case, the variation of the SFG and SHG of

the cw laser increases with the growth of the pump power of the cw laser; however, the SHG of the ps laser shows opposite variation tendency due to energy transportation from the pulse pump to the SFG.

4. CONCLUSIONS

In conclusion, we demonstrated SFG in on-chip LN microdisk resonators for the first time, to the best of our knowledge. The SFG signal commonly accompanied by SHG signals was generated by simultaneously pumping the LN resonator with a cw laser and a ps laser operating at different wavelengths. We investigated the influences of the experimental conditions, such as wavelength of the cw laser and the pump power, on the intensities of the SFG and SHG signals. This work not only expands the research field of nonlinear effects in micro- or nano-photonics devices but also paves the way for applications such as infrared single-photon detection and infrared spectroscopy based on on-chip LN microresonators.

Funding. National Natural Science Foundation of China (NSFC) (11374165, 11674181, 11674184, 61475077); Ministry of Science and Technology of the People's Republic of China (MOST) (2013CB328702); Ministry of Education of the People's Republic of China (MOE) (B07013); PCSIRT (IRT_13R29).

Acknowledgment. Z. Hao and J. Wang contributed equally to this work.

REFERENCES

1. J. Zhu, S. K. Ozdemir, Y.-F. Xiao, L. Li, L. He, D.-R. Chen, and L. Yang, "On-chip single nanoparticle detection and sizing by mode splitting in an ultrahigh-Q microresonator," Nat. Photonics **4**, 46–49 (2010).
2. L. He, S. K. Ozdemir, J. Zhu, W. Kim, and L. Yang, "Detecting single viruses and nanoparticles using whispering gallery microlasers," Nat. Nanotechnol. **6**, 428–432 (2011).
3. L. Shao, X. F. Jiang, X. C. Yu, B. B. Li, W. R. Clements, F. Vollmer, W. Wang, Y. F. Xiao, and Q. Gong, "Detection of single nanoparticles and lentiviruses using microcavity resonance broadening," Adv. Mater. **25**, 5616–5620 (2013).
4. L. He, S. K. Ozdemir, and L. Yang, "Whispering gallery microcavity lasers," Laser Photon. Rev. **7**, 60–82 (2013).
5. M. Asano, S. Komori, R. Ikuta, N. Imoto, S. K. Ozdemir, and T. Yamamoto, "Visible light emission from a silica microbottle resonator by second- and third-harmonic generation," Opt. Lett. **41**, 5793–5796 (2016).
6. V. S. Ilchenko, A. A. Savchenkov, A. B. Matsko, and L. Maleki, "Nonlinear optics and crystalline whispering gallery mode cavities," Phys. Rev. Lett. **92**, 043903 (2004).
7. J. U. Furst, D. V. Strekalov, D. Elser, M. Lassen, U. L. Andersen, C. Marquardt, and G. Leuchs, "Naturally phase-matched second-harmonic generation in a whispering-gallery-mode resonator," Phys. Rev. Lett. **104**, 153901 (2010).
8. V. S. Dmitry, S. K. Abijith, H. Yu-Ping, and K. Prem, "Optical sum-frequency generation in a whispering-gallery-mode resonator," New J. Phys. **16**, 053025 (2014).
9. J. U. Fürst, D. V. Strekalov, D. Elser, A. Aiello, U. L. Andersen, C. Marquardt, and G. Leuchs, "Low-threshold optical parametric oscillations in a whispering gallery mode resonator," Phys. Rev. Lett. **105**, 263904 (2010).
10. T. Beckmann, H. Linnenbank, H. Steigerwald, B. Sturman, D. Haertle, K. Buse, and I. Breunig, "Highly tunable low-threshold optical parametric oscillation in radially poled whispering gallery resonators," Phys. Rev. Lett. **106**, 143903 (2011).
11. T. Aoki, B. Dayan, E. Wilcut, W. P. Bowen, A. S. Parkins, T. J. Kippenberg, K. J. Vahala, and H. J. Kimble, "Observation of strong coupling between one atom and a monolithic microresonator," Nature **443**, 671–674 (2006).
12. T. J. Kippenberg and K. J. Vahala, "Cavity optomechanics: back-action at the mesoscale," Science **321**, 1172–1176 (2008).
13. C. Dong, V. Fiore, M. C. Kuzyk, and H. Wang, "Optomechanical dark mode," Science **338**, 1609–1613 (2012).
14. B. Peng, S. K. Ozdemir, F. Lei, F. Monifi, M. Gianfreda, G. L. Long, S. Fan, F. Nori, C. M. Bender, and L. Yang, "Parity-time-symmetric whispering-gallery microcavities," Nat. Phys. **10**, 394–398 (2014).
15. B. Peng, S. K. Ozdemir, S. Rotter, H. Yilmaz, M. Liertzer, F. Monifi, C. M. Bender, F. Nori, and L. Yang, "Loss-induced suppression and revival of lasing," Science **346**, 328–332 (2014).
16. M. Hafezi, E. A. Demler, M. D. Lukin, and J. M. Taylor, "Robust optical delay lines with topological protection," Nat. Phys. **7**, 907–912 (2011).
17. C.-H. Dong, Z. Shen, C.-L. Zou, Y.-L. Zhang, W. Fu, and G.-C. Guo, "Brillouin-scattering-induced transparency and non-reciprocal light storage," Nat. Commun. **6**, 6193 (2015).
18. S. Hua, J. Wen, X. Jiang, Q. Hua, L. Jiang, and M. Xiao, "Demonstration of a chip-based optical isolator with parametric amplification," Nat. Commun. **7**, 13657 (2016).
19. T. J. Kippenberg, R. Holzwarth, and S. A. Diddams, "Microresonator-based optical frequency combs," Science **332**, 555–559 (2011).
20. C. Y. J. Ying, C. L. Sones, A. C. Peacock, F. Johann, E. Soergel, R. W. Eason, M. N. Zervas, and S. Mailis, "Ultra-smooth lithium niobate photonic micro-structures by surface tension reshaping," Opt. Express **18**, 11508–11513 (2010).
21. T.-J. Wang, J.-Y. He, C.-A. Lee, and H. Niu, "High-quality $LiNbO_3$ microdisk resonators by undercut etching and surface tension reshaping," Opt. Express **20**, 28119–28124 (2012).
22. J. Lin, Y. Xu, Z. Fang, M. Wang, J. Song, N. Wang, L. Qiao, W. Fang, and Y. Cheng, "Fabrication of high-Q lithium niobate microresonators using femtosecond laser micromachining," Sci. Rep. **5**, 8072 (2015).
23. C. Wang, M. J. Burek, Z. Lin, H. A. Atikian, V. Venkataraman, I. C. Huang, P. Stark, and M. Loncar, "Integrated high quality factor lithium niobate microdisk resonators," Opt. Express **22**, 30924–30933 (2014).
24. R. Wang and S. A. Bhave, "Free-standing high quality factor thin-film lithium niobate micro-photonic disk resonators," arXiv:1409.6351 (2014).
25. J. Wang, F. Bo, S. Wan, W. Li, F. Gao, J. Li, G. Zhang, and J. Xu, "High-Q lithium niobate microdisk resonators on a chip for efficient electro-optic modulation," Opt. Express **23**, 23072–23078 (2015).
26. J. Lin, Y. Xu, Z. Fang, M. Wang, N. Wang, L. Qiao, W. Fang, and Y. Cheng, "Second harmonic generation in a high-Q lithium niobate microresonator fabricated by femtosecond laser micromachining," Sci. China Phys. Mech. Astron. **58**, 114209 (2015).
27. J. Lin, Y. Xu, J. Ni, M. Wang, Z. Fang, L. Qiao, W. Fang, and Y. Cheng, "Phase-matched second-harmonic generation in an on-chip $LiNbO_3$ microresonator," Phys. Rev. Appl. **6**, 014002 (2016).
28. J. Moore, J. K. Douglas, I. W. Frank, T. A. Friedmann, R. Camacho, and M. Eichenfield, "Efficient second harmonic generation in lithium niobate on insulator," in *Conference on Lasers and Electro-Optics (CLEO)* (Optical Society of America, 2016), paper STh3P.1.
29. I. W. Frank, J. Moore, J. K. Douglas, R. Camacho, and M. Eichenfield, "Entangled photon generation in lithium niobate microdisk resonators through spontaneous parametric down conversion," in *Conference on Lasers and Electro-Optics (CLEO)* (Optical Society of America, 2016), paper SM2E.6.
30. M. Wang, Y. Xu, Z. Fang, Y. Liao, P. Wang, W. Chu, L. Qiao, J. Lin, W. Fang, and Y. Cheng, "On-chip electro-optic tuning of a lithium niobate microresonator with integrated in-plane microelectrodes," Opt. Express **25**, 124–129 (2017).
31. H. Liang, W. C. Jiang, X. B. Sun, X. C. Zhang, and Q. Lin, "Thermo-optic oscillation dynamics in a high-Q lithium niobate microresonator,"

in *Conference on Lasers and Electro-Optics (CLEO)* (Optical Society of America, 2016), paper STu1E.4.
32. J. Wang, B. Zhu, Z. Hao, F. Bo, X. Wang, F. Gao, Y. Li, G. Zhang, and J. Xu, "Thermo-optic effects in on-chip lithium niobate microdisk resonators," Opt. Express **24**, 21869–21879 (2016).
33. W. C. Jiang and Q. Lin, "Chip-scale cavity optomechanics in lithium niobate," Sci. Rep. **6**, 36920 (2016).
34. A. Rodriguez, M. Soljacic, J. D. Joannopoulos, and S. G. Johnson, "$\chi^{(2)}$ and $\chi^{(3)}$ harmonic generation at a critical power in inhomogeneous doubly resonant cavities," Opt. Express **15**, 7303–7318 (2007).